Synergy of aromatic residues and phosphoserines within the intrinsically disordered DNA-binding inhibitory elements of the Ets-1 transcription factor

Geneviève Desjardins[a], Charles A. Meeker[b], Niraja Bhachech[b], Simon L. Currie[b], Mark Okon[a], Barbara J. Graves[b,c,1], and Lawrence P. McIntosh[a,1]

[a]Department of Biochemistry and Molecular Biology, Department of Chemistry, and Michael Smith Laboratories, University of British Columbia, Vancouver, BC, Canada V6T 1Z3; [b]Department of Oncological Sciences, University of Utah School of Medicine, Huntsman Cancer Institute, University of Utah, Salt Lake City, UT 84112; and [c]Howard Hughes Medical Institute, Chevy Chase, MD 20815

Edited* by Steven L. McKnight, The University of Texas Southwestern Medical Center, Dallas, TX, and approved June 20, 2014 (received for review January 29, 2014)

The E26 transformation-specific (Ets-1) transcription factor is autoinhibited by a conformationally disordered serine-rich region (SRR) that transiently interacts with its DNA-binding ETS domain. In response to calcium signaling, autoinhibition is reinforced by calmodulin-dependent kinase II phosphorylation of serines within the SRR. Using mutagenesis and quantitative DNA-binding measurements, we demonstrate that phosphorylation-enhanced autoinhibition requires the presence of phenylalanine or tyrosine (ϕ) residues adjacent to the SRR phosphoacceptor serines. The introduction of additional phosphorylated Ser-ϕ-Asp, but not Ser-Ala-Asp, repeats within the SRR dramatically reinforces autoinhibition. NMR spectroscopic studies of phosphorylated and mutated SRR variants, both within their native context and as separate *trans*-acting peptides, confirmed that the aromatic residues and phosphoserines contribute to the formation of a dynamic complex with the ETS domain. Complementary NMR studies also identified the SRR-interacting surface of the ETS domain, which encompasses its positively charged DNA-recognition interface and an adjacent region of neutral polar and nonpolar residues. Collectively, these studies highlight the role of aromatic residues and their synergy with phosphoserines in an intrinsically disordered regulatory sequence that integrates cellular signaling and gene expression.

transcription factor regulation | protein dynamics | intrinsically disordered region | fuzz complex

Intrinsically disordered protein regions (IDRs) are increasingly recognized for their prevalence in the eukaryotic proteome and their roles in normal biological processes, as well as in disease (1–3). IDRs serve as flexible linker sequences between modular domains and as key components of complex protein-interaction networks. These sequences are often sites of posttranslational modifications, and their plasticity enables accessible and reversible interactions necessary for the integration of cellular signals.

The autoinhibition of the E26 transformation-specific (Ets-1) transcription factor provides an illuminating example of how a flexible, disordered region can modulate the regulatable DNA-binding ETS domain and thereby tune it for biological control by calcium-dependent phosphorylation and cooperative protein partnerships (4). The inhibitory module (IM) of Ets-1 is composed of four α-helices (HI-1, HI-2, H4, and H5) that pack onto the ETS domain distal from the DNA interface (Fig. 1*A*) (5). Helix HI-1 is marginally stable and unfolds on DNA binding, thus implicating an allosteric mechanism of inhibition (6, 7). The modest twofold repression afforded by the IM is increased to ∼20-fold by an intrinsically disordered serine-rich region (SRR) (8, 9). The dynamic SRR interacts transiently with both the ETS domain DNA-binding interface and the IM, and thus plays steric and allosteric inhibitory roles (10). Phosphorylation of five SRR serines by calmodulin-dependent kinase II (CaMKII) leads to a dramatic ∼500-fold autoinhibition (11). In parallel, the conformational flexibility of the IM, and the ETS domain decreases (9, 10). By analogy to the well-characterized lac repressor (12), this flexibility is hypothesized to play a central role in DNA binding.

This study interrogates the physicochemical basis of the transient interactions underpinning Ets-1 autoinhibition. Through mutational analyses, we found that Phe/Tyr (ϕ) residues in the SRR act synergistically with nearby phosphoserines to reinforce autoinhibition. Complementing these biochemical assays, we used NMR spectroscopy to investigate the intermolecular interactions of peptides, corresponding to the SRR, with the IM and ETS domain. The *trans*-SRR peptides retained inhibitory activity and formed dynamic complexes, lacking any persistent induced conformation, via the same interface detected "in *cis*" by chemical shift perturbation (CSP) and paramagnetic relaxation enhancement (PRE) experiments. Intermolecular binding was also enhanced by phosphorylation and weakened on alanine substitution of the Phe/Tyr residues. These studies revealed the synergy between aromatic residues and phosphoserines in the function of an IDR.

Results

Aromatics Are Essential for Phosphorylation-Enhanced Autoinhibition. Sequence alignment of the SRR, which is unique to Ets-1 and Ets-2, revealed a repetitive pattern of Phe/Tyr and Asp/Glu residues adjacent to the CaMKII phosphoacceptors (Fig. 1*A* and Fig. S1). We tested the roles of these conserved residues

Significance

Eukaryotic proteins often contain intrinsically disordered regions that lack well-defined conformations, yet still play key roles in numerous biological processes. The molecular mechanisms underlying the functions of such unstructured regions are often poorly understood. In the case of the E26 transformation-specific transcription factor, DNA binding by the ETS domain is autoinhibited through transient interactions with an adjacent disordered serine-rich region (SRR). Phosphorylation of the SRR in response to cellular signals increases these interactions and thereby reinforces autoinhibition. In this study, we demonstrate that phosphorylation-enhanced autoinhibition requires the presence of phenylalanine or tyrosine residues neighboring the SRR phosphoacceptor serines. This highlights a previously unrecognized role of aromatic residues and their synergy with phosphoserines in an intrinsically disordered regulatory sequence.

Author contributions: G.D., C.A.M., N.B., S.L.C., M.O., B.J.G., and L.P.M. designed research; G.D., C.A.M., N.B., S.L.C., and M.O. performed research; G.D., C.A.M., N.B., S.L.C., and M.O. analyzed data; and G.D., B.J.G., and L.P.M. wrote the paper.

The authors declare no conflict of interest.

*This Direct Submission article had a prearranged editor.

[1]To whom correspondence may be addressed. Email: barbara.graves@hci.utah.edu or mcintosh@chem.ubc.ca.

This article contains supporting information online at www.pnas.org/lookup/suppl/doi:10.1073/pnas.1401891111/-/DCSupplemental.

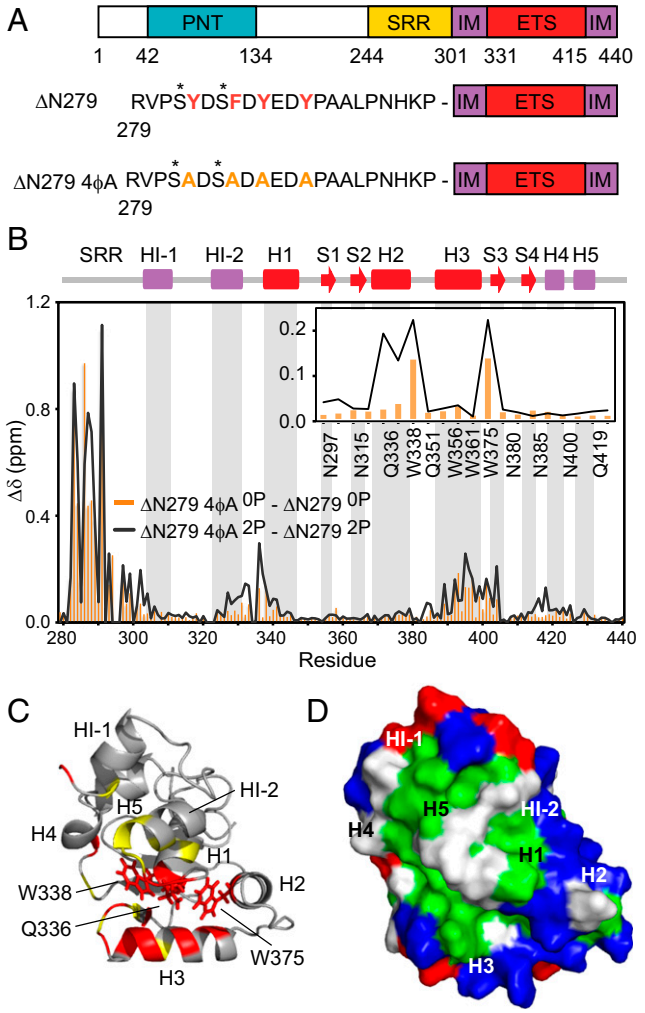

Fig. 1. Intramolecular interactions of the SRR with the ETS domain are dependent on aromatic residues and phosphoserines. (*A*) Ets-1 schematic: PNT domain (cyan), SRR (yellow), IM (purple), ETS domain (red). ΔN279 with SRR residues, CaMKII phosphoacceptors S282 and S285 (*), and four mutated aromatic residues (4ϕA; red, orange). (*B*) CSPs for main-chain amides and side-chain amides/indoles (*Inset*) in ΔN279 (orange bars) and $\Delta N279^{2P}$ (black lines) on 4ϕA substitutions. See Fig. S2*A* for other comparisons. (*C*) CSPs for residues 301–440 of $\Delta N279^{2P}$ on 4ϕA mutation mapped on ΔN301 [Protein Data Bank (PDB) ID 1R36] with perturbed side chains in stick format (red: $\Delta\delta > 0.125$ ppm, yellow: $0.125 \text{ ppm} > \Delta\delta > 0.08$ ppm, gray: $\Delta\delta < 0.08$ ppm or prolines). (*D*) Surface representation of ΔN301 showing the positively charged (blue; Arg, Lys), negatively charged (red; Asp, Glu), hydrophobic (green), and neutral polar (white) residues.

using ΔN279, an Ets-1 species with a shorter SRR that retains phosphorylation-dependent autoinhibition. Consistent with previous studies (9, 10), the truncated SRR caused 18-fold inhibition of DNA binding for ΔN279 relative to ΔN301 (only the IM and ETS domain), and phosphorylation of S282 and S285 increased this to 1,900-fold (Table 1). Serine substitution with glutamates or aspartates increased inhibition to only ~75-fold. The partial effects of these phosphomimetics may arise from charge (−2 vs. −1 at pH 8) and/or structural differences. Lowering the SRR net negative charge by substitution of D284, D287, E289, and D290 with alanines did not alter basal autoinhibition. (CaMKII failed to phosphorylate these mutants, and thus effects on the reinforcement of autoinhibition could not be measured.) Replacing the negative charges of the added phosphates with positive charges via arginine substitutions at S282 and S285 also failed to reinforce autoinhibition. These findings indicated that the SRR does not act by a simple global electrostatic effect, but rather through a specific role of the phosphoserines.

Next, four conserved aromatic residues in the SRR were investigated (Table 1). Alanine (or glycine) substitutions reduced phosphorylation-dependent inhibition to only approximately threefold for $\Delta N279\text{-}4\phi A^{2P}$ vs. $\Delta N279\text{-}4\phi A^{0P}$ compared with an ~100-fold effect for the corresponding WT species, while showing minimal effects on basal inhibition. Similar results were found in mutational tests of ΔN244 and native Ets-1, which have the full SRR with five phosphoacceptor serines. Substitution of the four aromatics in ΔN279 to valines had comparable effects to alanine replacements, strongly suggesting that the aromatic character of tyrosines and phenylalanines is essential for phosphorylation-dependent inhibition. The importance of phosphorylated serines and aromatic residues within a possible repeating unit was tested with SRR variants containing one, two, or four additional Ser-ϕ-Asp repeats (Table 2). Although there was only a minimal effect on basal inhibition, phosphorylation weakened DNA binding up to 10,000-fold. In contrast, Ser-Ala-Asp repeats lacking aromatics were ineffective even in the highly phosphorylated state. We conclude that the phosphoserines and aromatic residues contribute synergistically to autoinhibition.

Aromatic Residues and Phosphorylation Mediate Intramolecular Interactions. CSP and ^{15}N relaxation measurements probed the conformation and intramolecular interactions of the 4ϕA version of the ΔN279 SRR. A comparison of the ^{15}N-heteronuclear single quantum correlation (HSQC) spectra of WT and the 4ϕA mutant showed the largest CSPs were within the SRR (Fig. 1*B*). Importantly, amides within the ETS domain and IM also exhibited small CSPs. Phosphorylation of either WT or the 4ϕA mutant also led to similar patterns of CSPs (Fig. S2*A*). However, these spectral perturbations were generally larger on phosphorylation of WT than the 4ϕA mutant and on mutation of the phosphorylated rather than the nonphosphorylated protein. When mapped onto the ΔN301 structure, residues with the largest CSPs clustered near helix H3 and the following β-strand S4 of the ETS domain, as well as in the HI-2/H1 and S4/H4 loops (Fig. 1*C*). This surface is very similar to that detected by PRE measurements of WT ΔN279 with a nitroxide spin label covalently linked to Cys278 (Fig. S2 *B* and *C*). These NMR approaches defined the aromatic- and phosphoserine-dependent interface, including positively charged residues near the DNA interface, as well as an adjacent patch of hydrophobic and neutral polar residues. Thus, both

Table 1. Mutations demonstrate a critical role for SRR aromatics in phosphorylation-enhanced autoinhibition of ΔN279 DNA binding

Protein	SRR sequence*	K_D (×10^{-11} M)†	Fold inhibition†
ΔN301		2.5 ± 0.5	—
$\Delta N279^{0P}$	RVPS YDS FDYEDYP	44 ± 4.4	18 ± 2.7
$\Delta N279^{2P}$	RVP**S^P**YD**S^P**FDYEDYP	4,700 ± 580	1,900 ± 320
$\Delta N279^{0P}$ S➤E	RVP**E** YD**E** FDYEDYP	180 ± 50	73 ± 27
$\Delta N279^{0P}$ S➤D	RVP**D** YD**D** FDYEDYP	190 ± 7.8	77 ± 9.8
$\Delta N279^{0P}$ DE➤A	RVPS YA**A**S FA**A**YA**A**YP	71 ± 16	28 ± 8.5
$\Delta N279^{0P}$ S➤R	RVP**R** YD**R** FDYEDYP	45 ± 4.9	18 ± 2.7
$\Delta N279\ 4\phi G^{0P}$	RVPS **G**DS **G**D**G**ED**G**P	44 ± 8.7	18 ± 4.0
$\Delta N279\ 4\phi G^{2P}$	RVP**S^{P}G**D**S^{P}G**D**G**ED**G**P	130 ± 11	50 ± 7.2
$\Delta N279\ 4\phi A^{0P}$	RVPS **A**DS **A**D**A**ED**A**P	44 ± 1.7	18 ± 2.2
$\Delta N279\ 4\phi A^{2P}$	RVP**S^{P}A**D**S^{P}A**D**A**ED**A**P	140 ± 10	54 ± 7.5
$\Delta N279\ 4\phi V^{0P}$	RVPS **V**DS **V**D**V**ED**V**P	23 ± 2	9 ± 2
$\Delta N279\ 4\phi V^{2P}$	RVP**S^{P}V**D**S^{P}V**D**V**ED**V**P	160 ± 33	63 ± 18

*Phosphoserines (S^P) and mutated/modified sites are bold underlined.
†Measured by EMSA for a consensus Ets-1 site. Inhibition relative to ΔN301.

Table 2. Additional Ser-ϕ-Asp repeats mediate higher levels of phosphorylation-dependent autoinhibition of ΔN279 DNA binding

Protein	SRR sequence*	K_D ($\times 10^{-11}$ M)†	Fold inhibition†
$\Delta N279^{0P}$	RVP-S YD-S FD-Y ED-Y PA-A LP-N HK-P	44 ± 4.4	18 ± 2.7
$\Delta N279^{2P}$	RVP-**S^P**YD-**S^P**FD-Y ED-Y PA-A LP-N HK-P	4,700 ± 580	1,900 ± 320
3-unit SRR^{0P}	RVP-S YD-S FD-**S YD**-Y PA-A LP-N HK-P	44 ± 3.8	18 ± 2.2
3-unit SRR^{2P}	RVP-**S^P**YD-**S^P**FD-**S^PYD**-Y PA-A LP-N HK-P	5,900 ± 2,700	2,400 ± 1,200
4-unit SRR^{0P}	RVP-S YD-S FD-**S YD**-**S FD**-A LP-N HK-P	51 ± 1.7	20 ± 2.5
4-unit SRR^{4P}	RVP-**S^P**YD-**S^P**FD-**S^PYD**-**S^PFD**-A LP-N HK-P	33,000 ± 17,000	13,000 ± 5,700
6-unit SRR^{0P}	RVP-S YD-S FD-**S YD**-**S FD**-**S YD**-**S FD**-P	58 ± 17	23 ± 7.0
6-unit SRR^{6P}	RVP-**S^P**YD-**S^P**FD-**S^PYD**-**S^PFD**-**S^PYD**-**S^PFD**-P	> 200,000	> 100,000
6-unit $4\phi A^{0P}$	RVP-S **A**D-S **A**D-**S AD**-**S AD**-**S AD**-**S AD**-P	40 ± 4.4	16 ± 2.6
6-unit $4\phi A^{6P}$	RVP-**S^PA**D-**S^PA**D-**S^PAD**-**S^PAD**-**S^PAD**-**S^PAD**-P	210 ± 46	84 ± 21

*Constructs for tandem repeats, delineated by hyphenation, retained WT SRR length by replacing 3, 6, or 12 amino acids. Phosphoserines (S^P) and mutated/modified sites are bold underlined.
†Measured by EMSA for a consensus Ets-1 site. Fold inhibition relative to ΔN301 (Table 1).

electrostatic and hydrophobic/van der Waals forces contribute to the SRR-ETS domain interactions (Fig. 1*D*).

The fast subnanosecond timescale backbone motions of the mutant SRR-4ϕA in the context of ΔN279 were also investigated by $^1H\{^{15}N\}$-nuclear Overhauser effect (NOE) measurements (Fig. S3). In both the unmodified and phosphorylated forms, the SRR-4ϕA residues showed significantly lower amide NOE values, and hence greater mobility, than residues in the ordered regions of the protein. However, the NOE values of residues throughout the SRR-4ϕA increased on phosphorylation. Consistent with a previous ^{15}N relaxation analysis of the WT ΔN279 (10), we conclude that the SRR functions through intramolecular interactions with the ETS domain and inhibitory elements and that its dynamic character scales inversely with its phosphorylation-dependent inhibitory activity.

***Trans*-SRR System Recapitulates Autoinhibition.** We developed a *trans* system wherein ΔN279 is represented by a SRR peptide and ΔN301 (Fig. 2*A*). The intermolecular system opened the door to new concentration-dependent structural studies of the SRR. Addition of a peptide version of the phosphorylated SRR^{2P} weakened binding of ΔN301 to DNA (Fig. S4), whereas peptides that either lacked phosphoserines, or had the 4ϕA mutations, failed to measurably inhibit in *trans*. In NMR-monitored titrations (Table 3, Fig. 2*B*, and Fig. S5*A*), the SRR^{2P} peptide showed the highest affinity for ΔN301 with an equilibrium dissociation constant (K_D) of 100 μM. The absence of the two phosphates in SRR^{0P} caused a 16-fold affinity reduction (K_D ~ 1,650 μM). Increasing ionic strength from 50 to 200 mM NaCl reduced the affinity of both SRR^{0P} and SRR^{2P} peptides for ΔN301 by a modest two- to threefold, indicating an electrostatic component to binding. Replacing the four aromatic residues in the SRR peptide with alanines (SRR-$4\phi A^{0P}$) severely weakened binding, precluding reliable K_D measurement. Phosphorylation of the mutant SRR-$4\phi A^{2P}$ peptide partially restored its affinity for ΔN301 (K_D ~ 260 μM). Thus, the SRR peptides recapitulated the *cis*-acting inhibitory properties of ΔN279.

To identify the residues of the SRR that interact with ΔN301, we titrated the WT $^{13}C/^{15}N$-labeled peptides with unlabeled protein (Fig. 3 *A* and *B* and Fig. S6). The amides of D284, S285, F286, Y288, and E289, as well as the aromatic nuclei of F286, exhibited chemical shift changes on addition of ΔN301 to SRR^{0P}. In the case of the SRR^{2P} peptide, backbone amide and side-chain aromatic nuclei of residues 283–291 inclusive showed larger CSPs, likely due to its higher affinity and hence increased saturation levels. Together, these titrations confirmed that *trans* binding to ΔN301 involves both phosphoserine and aromatic moieties within the SRR peptides.

We also used reciprocal NMR-monitored titrations to determine and compare the interaction surface of the four SRR peptides on ΔN301. Addition of each to the ^{15}N-labeled protein led to similar patterns of CSPs, albeit with varying magnitudes due, at least in part to differing affinities that precluded the formation of the fully saturated complexes (Fig. 4 and Fig. S5 *B* and *C*). Residues of ΔN301 showing the largest CSPs clustered within the loop between helices HI-2 and H1 linking the IM to the ETS domain, as well as within H3 and strand S3 of the ETS domain. On more detailed inspection, amides near the C terminus of H3 and in the loop to S3 (including W338, L341, and K399) showed colinear CSPs when titrated with the four peptides (Fig. 4). These spectral changes might arise from common local conformational perturbations linked to autoinhibition. A similar phenomenon of colinear CSPs paralleling DNA-binding affinity is seen with *cis*-acting SRR variants (9). In contrast, for

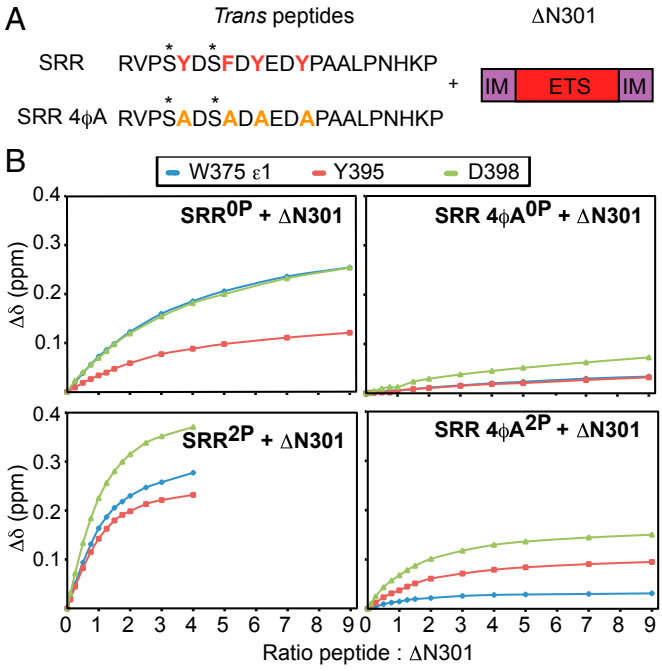

Fig. 2. Intermolecular interactions of the *trans*-SRR peptides with the ETS domain are dependent on adjacent aromatic residues and phosphoserines. (*A*) SRR peptides (residues 279–300) and ΔN301. (*B*) SRR peptide affinities were obtained by fitting the NMR chemical shift changes (data points) of perturbed ΔN301 nuclei. See Table 3 for K_D values and Fig. S5*A* for full spectra.

BIOCHEMISTRY

Table 3. Dissociation constants (K_D) for the *trans*-SRR peptides with ΔN301

Peptide	50 mM NaCl	90 mM NaCl	200 mM NaCl
SRR^{0P}	1,650 ± 250 μM	3,300 ± 1000 μM	
SRR^{2P}	100 ± 10 μM	150 ± 20 μM	350 ± 40 μM
SRR-4ϕA^{0P}	—*		
SRR-4ϕA^{2P}	260 ± 30 μM		

K_D values ± SEs were obtained by averaging the individual fit values of seven perturbed residues (L393, R394, Y395, Y396, D398, I401, $W338^{\varepsilon 1}$, and $W375^{\varepsilon 1}$).

*Although binding weakly, a reliable K_D value could not be measured.

other residues (including L337, W375, and Y395) clustering near the N terminus of H3 and the H2-H3 turn, the CSP patterns differed for SRR-4ϕA^{0P} and SRR-4ϕA^{2P} relative to SRR^{0P} and SRR^{2P}. These differences might reflect CSPs due to aromatic ring currents, thus suggesting that the SRR aromatic residues localize to this region of ΔN301. Overall, the same surface regions were identified for the intramolecular interactions within ΔN279 by PRE and CSP studies (Figs. S2 and S7). Thus, the interactions of the *trans*-peptides recapitulate the intramolecular allosteric and steric mechanisms of SRR-mediated autoinhibition.

***Trans*-SRR Peptides Are Intrinsically Disordered and Form Dynamic Complexes with ΔN301.** We probed the conformational and dynamic properties of the SRR peptides to pursue further how aromatic residues and phosphorylation contribute to autoinhibition. The secondary structural propensities of the SRR peptides were predicted by analysis of main-chain chemical shifts with the algorithm δ2D (13) (Fig. 3*C* and Fig. S8*A*). Consistent with their limited spectral dispersion, both the unmodified SRR^{0P} and phosphorylated SRR^{2P} peptides showed almost identical high random coil propensities (Fig. S6). This confirms that they are predominantly disordered and that phosphorylation does not induce any persistent secondary structure. When bound to ΔN301, the SRR^{2P} peptide also exhibited random coil chemical shifts, with only a slightly higher propensity for residues 283–287 to sample extended conformations (Fig. S8*A*). Therefore, the *trans*-peptides form dynamic complexes with the ETS domain. This is consistent with the previously described behavior of the flexible SRR in ΔN279 (Fig. S8*B*) (9, 10).

The ^{15}N-HSQC spectra of the SRR peptides, as well as the SRR residues in the context of ΔN279 (10), also contained a subset of weaker signals arising from conformers with significant populations of *cis* X-Pro amide bonds (Fig. 3*A*, Fig. S6, and Table S1). Phosphorylation did not markedly change the conformational equilibria of the prolines. The weaker signals also shifted on titration with ΔN301 and had a high random coil propensity in the bound state. Thus, ΔN301 interacts with the SRR peptides with either *trans* or *cis* X-Pro conformations. This provides further evidence for dynamic complexes.

The fast subnanosecond timescale dynamics of the unbound SRR peptides were investigated by ^{1}H{^{15}N}-NOE measurements (Fig. 3*D*). In the case of SRR^{0P} peptide, the terminal residues are very dynamic, with NOE values less than −0.75. However, the central residues, which mediate binding to ΔN301, exhibited values around zero. Thus, although lacking any predominant secondary structure, the motions of the SRR^{0P} peptide backbone are partially dampened. The phosphorylated SRR^{2P} peptide showed slightly higher NOE values for these central residues, suggesting a small reduction in mobility. More strikingly, the NOE values of residues throughout SRR-4ϕA^{0P} decreased substantially to those more characteristic of a random coil polypeptide (14, 15). This indicates that the presence of the four aromatic sidechains dampens the backbone flexibility of the SRR peptides, possibly through the formation of dynamic hydrophobic clusters that lack any persistent secondary structure. This also provides a possible mechanism for the synergy between phosphoserines and aromatic residues.

Discussion

Aromatic Residues in the SRR Are Critical for Phosphorylation-Dependent Autoinhibition. Previous studies demonstrated that the intrinsically disordered SRR is required for both basal and phosphorylation-enhanced autoinhibition of Ets-1 DNA binding, yet the underlying molecular interactions were largely unknown. IDRs are generally depleted in hydrophobic amino acids (16), and thus it is striking that the CaMKII phosphoacceptor serines contributing to autoinhibition are adjacent to Phe/Tyr (ϕ) residues within a Ser-ϕ-Asp/Glu repeat. There are two repeats in the truncated SRR (^{282}-SYD-SFD-^{287}) and a third in the full SRR (^{251}-SFE-^{253}) (9, 11). Mutation of these two aromatic residues and two additional ones within the truncated SRR to glycines, alanines, or valines strongly reduced phosphorylation-enhanced autoinhibition. Conversely, the presence of additional Ser-ϕ-Asp repeats dramatically increased the effect, whereas even six phosphorylated Ser-Ala-Asp repeats did not reinforce autoinhibition. The contribution of the aromatic residues was confirmed using the *trans*-SRR system. On addition of ΔN301, NMR signals from the aromatic residues in the SRR peptides shifted, indicating that they are involved directly in the intermolecular interface. Furthermore, the SRR-4ϕA^{2P} peptide bound ΔN301 with approximately threefold lower affinity than did the SRR^{2P} peptide, and the very weak interaction of the SRR-4ϕA^{0P} peptide could not be quantified. Thus, both phosphoserines and adjacent Phe/Tyr residues within the SRR act synergistically to inhibit Ets-1 DNA binding.

Fuzzy Interactions Between the SRR and ETS Domain. The interactions between the SRR and ETS domain can be described as fuzzy based on their transient nature and the lack of any induced, persistent structure (17). This conclusion, which stands in sharp contrast to examples of disordered regions that fold into well-defined structures on partner binding, derives from several lines of evidence. Whether linked to the IM and ETS domain as in ΔN279 or as an isolated peptide, the SRR residues have random coil chemical shifts. Furthermore, neither phosphorylation nor ΔN301 binding causes any chemical shift changes indicative of a predominant induced structure. Amide ^{1}H{^{15}N}-NOE experiments also demonstrated that the residues in the SRR are significantly more flexible on a subnanosecond timescale than those in the well-ordered ETS domain. However, the backbone motions of the SRR are not unrestricted. Based on the substantially lower NOE values of the SRR-4ϕA peptide relative to the WT peptide, this might result from hydrophobic clustering of the four aromatic residues. The motions of the SRR also dampen with increased binding to the ETS domain on phosphorylation. Thus, the SRR appears to rapidly interconvert between an ensemble of conformations that are partially restrained by transient interactions, both within the SRR itself and with the ETS domain. This ensemble may involve binding of the flexible SRR at one predominant site or at multiple sites on the ETS domain. These two possibilities were not resolved due to coarse nature of CSP and PRE data and the absence of detectable interproton NOEs between the SRR and ETS domain (10).

The interaction surface of Ets-1 contacted by the SRR helps us understand how the dynamic complex functions in autoinhibition. This surface, which spans from the ETS domain to the IM, was broadly defined through NMR-monitored titrations of ΔN301 with the *trans*-SRR peptides, PREs from an N-terminal MTSL spin label on ΔN279, and CSPs of ΔN279 resulting from 4ϕA-mutation and phosphorylation of the SRR. Overall, this region has a net positive charge due to several Arg and Lys residues, whereas the SRR of ΔN279 contains four Asp and Glu residues, as well as two phosphoacceptor serines. Thus,

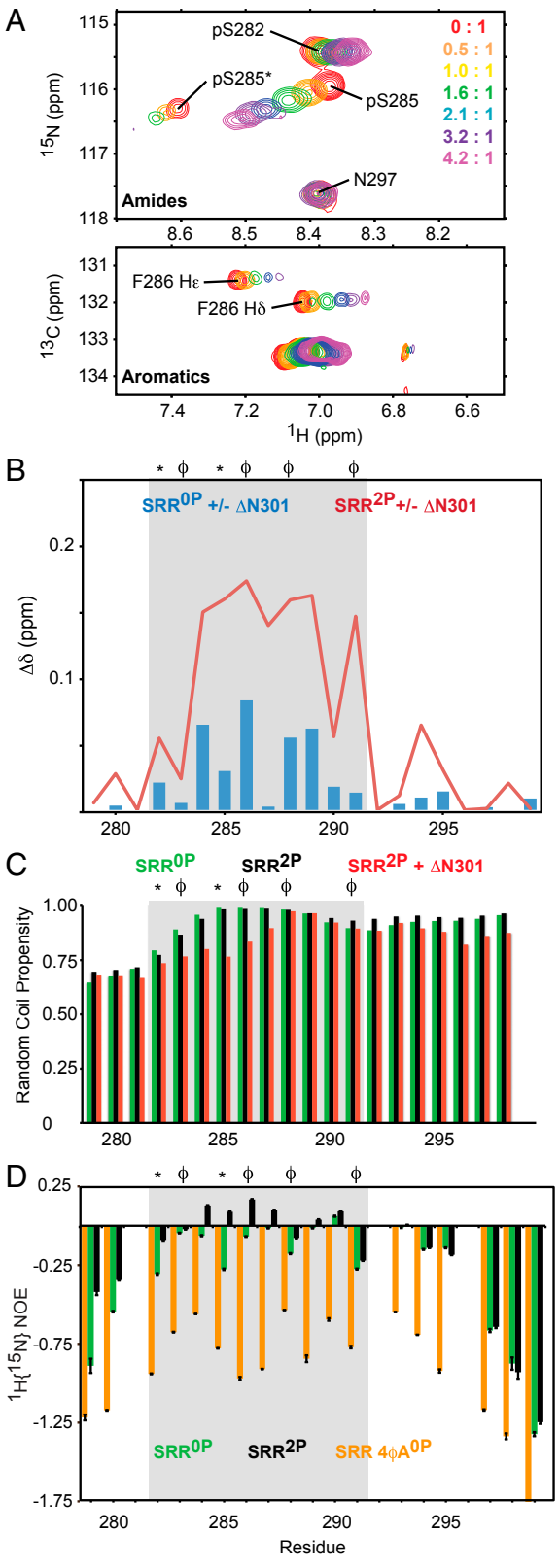

Fig. 3. Characterizing the *trans*-SRR peptide structure, dynamics and ΔN301-binding interface. (*A*) Overlaid ^{15}N-HSQC and ^{13}C-HSQC spectra of ^{13}C/^{15}N-labeled SRR^{2P} on progressive addition of unlabeled ΔN301 in the indicated protein:peptide molar ratios. pS285* is from a population of peptide with a *cis* Val280-Pro281 bond. See Fig. S6 for full spectra. (*B*) Amide CSPs observed upon addition of ΔN301 to the labeled SRR^{0P} (~25% saturation; blue bars) and SRR^{2P} (~85% saturation; red line). Peptide interface (gray), aromatic residues (ϕ), phosphoacceptors (*). (*C*) Propensities of the SRR^{0P} (green), SRR^{2P} (black), and ΔN301-bound SRR^{2P} (~85% saturation; red) to adopt random coil conformations, as calculated with δ2D (13) (*trans* X-Pro conformers shown, *cis* X-Pro yielded similar results; Fig. S8*A*). (*D*) ^{1}H{^{15}N}-NOE ratios for SRR^{0P} (green), SRR^{2P} (black), and SRR-4ϕA^{0P} (orange). Decreasing values indicate increasing flexibility on the subnanosecond timescale. Missing data are prolines or residues with overlapped signals.

electrostatic forces likely contribute to the interaction of the SRR with the ETS domain and IM. This conclusion is further supported by the modestly weakened K_D values of the SRR peptides for ΔN301 with increasing ionic strength. However, glutamate and aspartate are only partial mimics of phosphoserine, and removing the four carboxylates or introducing two arginines does not impair basal autoinhibition. Therefore, more than simple Coulombic interactions are at play. Indeed, the SRR-interacting surface of the Ets-1 ETS domain overlaps with a relatively large patch of neutral polar and nonpolar residues between the IM and DNA-recognition helix (Fig. 1*D*). With partially exposed side chains, Tyr307 (HI-1), Tyr329 (HI-2), Trp338 (H1), Tyr395 (H3), and Tyr396 (H3) are included in this patch. Thus, hydrophobic and van der Waals interactions involving aromatic residues could also help localize the SRR to this region of Ets-1.

Role of Aromatic Residues in IDRs. The observation that phosphorylation-enhanced autoinhibition requires the presence of aromatic residues suggests that the SRR functions through more than just a simple collection of weak electrostatic and hydrophobic/van der Waals contacts. What then are the underlying forces by which aromatic residues integrate with phosphoserines to mediate SRR-ETS domain binding? One possible mechanism could involve the simultaneous association of adjacent phosphoserines and aromatic residues with lysine and arginine sidechains in the DNA-recognition interface of Ets-1 via ion-pair and π/cation interactions, respectively (18, 19). This would result in cooperative, multivalent binding of the SRR with the ETS domain. Alternatively, the negatively charged phosphates could interact with solvent and help drive a hydrophobic clustering of the neighboring aromatic residues either within the SRR or with the hydrophobic residues on the surface of the ETS domain and the IM. In support of this hypothesis, as a "salting-out" anion in the Hofmeister series, phosphate decreases the solubility of nonpolar solutes and stabilizes proteins, possibly through the ordering of water (20–22).

Functionally critical aromatic groups in IDRs are also found in the disordered activation domain (EAD) of the transcription factor EWS/FLI. This ~280 residue region is a low complexity sequence comprised mainly of a repeating SYGQQS motif. The activity of the EAD in transcriptional regulation and oncogenesis is strongly dependent on the presence of multiple tyrosines within these repeats (23, 24). A structural contribution of the multiple tyrosines in the (G/S)Y(G/S) repeats of all related FET proteins (FUS, EWS, and TAF15) is also suggested by the reversible polymerization of these IDRs (25). This may mediate biological regulation because the tyrosines are essential for phosphorylation-regulated binding of the EAD to the C-terminal domain (CTD) of RNA polymerase II. Although the EAD tyrosines are hypothesized to form fuzzy polycation/π interactions with yet unidentified positively charged partner proteins (26), the molecular forces driving these processes, which show both similarities and differences to the autoinhibitory SRR of Ets-1, remain to be established.

ETS Factor Autoinhibition. The Ets-1 autoinhibitory mechanism has both common and distinct features relative to those exploited by other ETS transcription factors and thus provides a route to specificity within this group of proteins that otherwise share

BIOCHEMISTRY

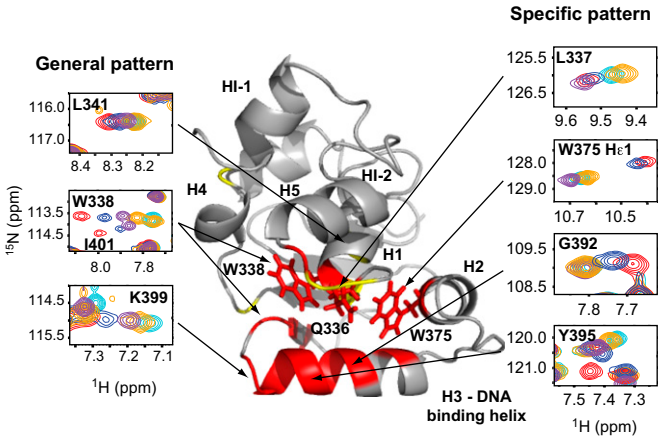

Fig. 4. *Trans*-SRR peptides interact with the ETS domain DNA-recognition interface of ΔN301. Small regions of the superimposed ^{15}N-HSQC spectra of ^{15}N-labeled ΔN301 (~250 μM) in the absence (cyan contours) or presence of SRR-4ϕA^{0P} (1.1-mM peptide yielding <37% saturation based on the K_D values of Table 3; orange), SRR-4ϕA^{2P} (1.1 mM, 78%; purple), SRR^{0P} (1.0 mM, 37%; blue), or SRR^{2P} (640 μM, 84%; red). Residues with large (>0.1 ppm; red) and medium (0.07–0.1 ppm; yellow) amide or indole CSPs on titration with SRR^{2P} are mapped on ΔN301 (PDB ID 1R36). Perturbed side chains in stick format. Other peptides were similar (Fig. S5 *B* and *C*). Residues (*Left*) exhibited a pattern of increasing shift perturbations in the order SRR-4ϕA^{0P} < SRR-4ϕA^{2P} < SRR^{0P} < SRR^{2P}, suggestive of similar structural perturbations. Residues (*Right*) showed peptide-specific changes.

highly related DNA-binding properties (4). Ets-related gene (ERG) is regulated by a dynamic N-terminal sequence that perturbs its DNA-binding helix in a manner akin to that of the Ets-1 SRR (27). However, this sequence is almost devoid of aromatic residues. Furthermore, ERG lacks an equivalent IM and is not known to be modulated at the level of DNA binding by phosphorylation. In contrast, ETV6 does not contain an equivalent SRR and instead is autoinhibited by a C-terminal helix that sterically blocks its ETS domain interface and unfolds upon binding both specific and nonspecific DNA sequences (28). In all of these cases, additional DNA binding proteins can counteract or bypass the negative effects of autoinhibition and thereby provide added specificity to each ETS factor.

Materials and Methods

The experimental procedures are provided in detail as *SI Materials and Methods*.

Sample Preparation. Unlabeled SRR peptides (N-terminal acetylated and C-terminal amidated) were synthesized with or without phosphoserine (Biomatik). Isotopically labeled peptides were expressed in *Escherichia coli* and isolated as glutathione S-transferase– and His$_6$-tagged fusions, followed by tag cleavage and reverse phase HPLC purification. Murine ΔN301 and ΔN279 variants were expressed in *E. coli*, isolated by multiple chromatographic steps (9, 10), and phosphorylated in vivo with CaMII kinase (9).

EMSAs. DNA-binding affinity of each Ets-1 variant was measured as previously described (9) with ^{32}P-labeled duplexed 27-mer oligonucleotides: 5′-TCGACGGCCAAGCC**GGAA**GTGAGTGCC-3′ (top strand; GGAA consensus noted in bold) and 5′-TCGAGGCACTCACTTCCGGCTTGGCCG-3′ (bottom strand). K_D values represent the average of at least two independent experiments ± SEM.

NMR Spectroscopy. Samples were in 20 mM Mes, 50 mM NaCl, 0.5 mM EDTA, 0.02% NaN_3, and 5 mM DTT with 5–10% (vol/vol) D_2O at pH 6.5. NMR data were recorded at 25 or 28 °C on 500- and 600-MHz spectrometers. Chemical shift perturbations were calculated from the combined ^{1}H and ^{15}N shift changes as $\Delta\delta = [(0.2 \times \Delta\delta_N)^2 + (\Delta\delta_H)^2]^{1/2}$. Peptide-protein titrations were monitored via sensitivity-enhanced ^{15}N-HSQC spectra, and K_D values determined by fitting Δδ to a 1:1 binding isotherm.

ACKNOWLEDGMENTS. This study was funded by Canadian Cancer Society Research Institute Grant 2011-700772 (to L.P.M.) and National Institutes of Health Grant R01 GM38663 (to B.J.G.). Instrument support was provided by the Canadian Institutes for Health Research (CIHR), the Canada Foundation for Innovation, the British Columbia Knowledge Development Fund, the University of British Columbia (UBC) Blusson Fund, and the Michael Smith Foundation for Health Research. Funding from the Huntsman Cancer Institute/Huntsman Cancer Foundation and the Howard Hughes Medical Institute is also acknowledged. G.D. held a CIHR Frederick-Banting Graduate Scholarship and a UBC Four Year Fellowship.

1. Dyson HJ, Wright PE (2005) Intrinsically unstructured proteins and their functions. *Nat Rev Mol Cell Biol* 6(3):197–208.
2. Dunker AK, Silman I, Uversky VN, Sussman JL (2008) Function and structure of inherently disordered proteins. *Curr Opin Struct Biol* 18(6):756–764.
3. Tompa P (2012) Intrinsically disordered proteins: A 10-year recap. *Trends Biochem Sci* 37(12):509–516.
4. Hollenhorst PC, McIntosh LP, Graves BJ (2011) Genomic and biochemical insights into the specificity of ETS transcription factors. *Annu Rev Biochem* 80:437–471.
5. Garvie CW, Pufall MA, Graves BJ, Wolberger C (2002) Structural analysis of the autoinhibition of Ets-1 and its role in protein partnerships. *J Biol Chem* 277(47):45529–45536.
6. Petersen JM, et al. (1995) Modulation of transcription factor Ets-1 DNA binding: DNA-induced unfolding of an alpha helix. *Science* 269(5232):1866–1869.
7. Lee GM, et al. (2005) The structural and dynamic basis of Ets-1 DNA binding autoinhibition. *J Biol Chem* 280(8):7088–7099.
8. Jonsen MD, Petersen JM, Xu QP, Graves BJ (1996) Characterization of the cooperative function of inhibitory sequences in Ets-1. *Mol Cell Biol* 16(5):2065–2073.
9. Pufall MA, et al. (2005) Variable control of Ets-1 DNA binding by multiple phosphates in an unstructured region. *Science* 309(5731):142–145.
10. Lee GM, et al. (2008) The affinity of Ets-1 for DNA is modulated by phosphorylation through transient interactions of an unstructured region. *J Mol Biol* 382(4):1014–1030.
11. Cowley DO, Graves BJ (2000) Phosphorylation represses Ets-1 DNA binding by reinforcing autoinhibition. *Genes Dev* 14(3):366–376.
12. Kalodimos CG, Boelens R, Kaptein R (2004) Toward an integrated model of protein-DNA recognition as inferred from NMR studies on the Lac repressor system. *Chem Rev* 104(8):3567–3586.
13. Camilloni C, De Simone A, Vranken WF, Vendruscolo M (2012) Determination of secondary structure populations in disordered states of proteins using nuclear magnetic resonance chemical shifts. *Biochemistry* 51(11):2224–2231.
14. Campbell AP, Spyracopoulos L, Irvin RT, Sykes BD (2000) Backbone dynamics of a bacterially expressed peptide from the receptor binding domain of *Pseudomonas aeruginosa* pilin strain PAK from heteronuclear ^{1}H-^{15}N NMR spectroscopy. *J Biomol NMR* 17(3):239–255.
15. Renner C, Schleicher M, Moroder L, Holak TA (2002) Practical aspects of the 2D ^{15}N-[^{1}H]-NOE experiment. *J Biomol NMR* 23(1):23–33.
16. Uversky VN, Dunker AK (2012) Multiparametric analysis of intrinsically disordered proteins: Looking at intrinsic disorder through compound eyes. *Anal Chem* 84(5):2096–2104.
17. Fuxreiter M (2012) Fuzziness: Linking regulation to protein dynamics. *Mol Biosyst* 8(1):168–177.
18. Crowley PB, Golovin A (2005) Cation-π interactions in protein-protein interfaces. *Proteins* 59(2):231–239.
19. Dougherty DA (2013) The cation-π interaction. *Acc Chem Res* 46(4):885–893.
20. von Hippel PH, Schleich T (1968) Ion effects on the solution structure of biological macromolecules. *Acc Chem Res* 2(9):257–265.
21. Baldwin RL (1996) How Hofmeister ion interactions affect protein stability. *Biophys J* 71(4):2056–2063.
22. Dill KA, Truskett TM, Vlachy V, Hribar-Lee B (2005) Modeling water, the hydrophobic effect, and ion solvation. *Annu Rev Biophys Biomol Struct* 34:173–199.
23. Ng KP, et al. (2007) Multiple aromatic side chains within a disordered structure are critical for transcription and transforming activity of EWS family oncoproteins. *Proc Natl Acad Sci USA* 104(2):479–484.
24. Lee KAW (2012) Molecular recognition by the EWS transcriptional activation domain. *Adv Exp Med Biol* 725:106–125.
25. Kwon I, et al. (2013) Phosphorylation-regulated binding of RNA polymerase II to fibrous polymers of low-complexity domains. *Cell* 155(5):1049–1060.
26. Song J, Ng SC, Tompa P, Lee KA, Chan HS (2013) Polycation-π interactions are a driving force for molecular recognition by an intrinsically disordered oncoprotein family. *PLOS Comput Biol* 9(9):e1003239.
27. Regan MC, et al. (2013) Structural and dynamic studies of the transcription factor ERG reveal DNA binding is allosterically autoinhibited. *Proc Natl Acad Sci USA* 110(33):13374–13379.
28. De S, et al. (2014) Steric mechanism of auto-inhibitory regulation of specific and non-specific DNA binding by the ETS transcriptional repressor ETV6. *J Mol Biol* 426(7):1390–1406.